engineering proceedings

MDPI

Proceeding Paper

Super Austenitic Stainless Steel with SiC Metal Matrix Composites for Nozzles in Harsh Environment †

Svetlana Boshnakova

Center of Competence "Smart Mechatronic, Eco- and Energy-Saving Systems and Technologies", Technical University Sofia, Branch Plovdiv, 4000 Plovdiv, Bulgaria; boshnakova.sv@bswins.com

† Presented at the 3rd International Electronic Conference on Machines and Applications, 12–14 May 2026; Available online: https://sciforum.net/event/IECMA2026.

Abstract

We investigated the possibility of developing super austenitic stainless steel Avesta SMO 254 X1NiCrMoCuN20-18-7 (EN 10088-4) and austenitic stainless steel X15CrNiSi25-21 (EN 10095) coated with SiC, resulting in the obtainment of a Metal Matrix Composite (MMC) by additive manufacturing (AM) for the upgrade of nozzles for sulfur recovery thermal reactors. One layer of the MMC targets the outer surface of the part that is in constant contact with the flame and the area is subjected to high friction erosion. The Directed Energy Deposition Laser (DED-LB) method has made it possible to produce a high strength-to-weight ratio. The aim is to engage lower-cost material with similar thermal stability and durability in extreme conditions. The robotic unit used for the application allowed for computer control of the positioning, feeding of the SiC particles inside the shielding gas and deposition in the molten pool. After the solidification process, visual testing (VT) and ultrasonic testing (UT) were applied for non-destructive evaluation, checking for disbonding and subsurface imperfections. Then, samples were tested with microhardness measurements, bond strength, microcracking detection, porosity, interface zone assessments and microstructural analysis. The process achieved 0.4 to 0.7 KJ mm^{-1} heat input with no defects and the intended nozzle surface passed UT and VT. Controlled parameters provided strong metallurgical bonding.

Keywords: additive manufacturing; directed energy deposition; corrosion

1. Introduction

Directed Energy Deposition based on Laser Beam (DED-LB) method, often referred to as laser cladding or laser metal deposition, has emerged as a pivotal technology in the industrial sector. Its primary advantage lies in the ability to deposit material directly onto existing components, making it an ideal solution for the manufacturing, repair, and restoration of high-value parts [1]. As a subset of additive manufacturing (AM), DED-LB ensures a superior metallurgical bond, providing structural integrity comparable to the base metal while offering high resistance to thermal and mechanical fatigue.

Unlike standard powder bed fusion methods, which are limited to building parts from scratch, DED-LB enables the direct application of high-quality material onto existing geometries. This flexibility is further enhanced by the multi-material integration capabilities, allowing for the creation of functionally graded layers or the application of specialized wear-resistant coatings (such as laser cladding and hardfacing) exclusively on critical zones. Furthermore, DED-LB offers a cost-effective intermediate solution; it can utilize relatively

Check for updates

Academic Editor: Stefano Mariani

Published: 7 September 2026

Copyright: © 2026 by the author. Licensee MDPI, Basel, Switzerland. This article is an open access article distributed under the terms and conditions of the Creative Commons Attribution (CC BY) license.

inexpensive powder-form feedstocks while maintaining a significantly smaller heat-affected zone (HAZ) compared to traditional welding and arc processes. This minimizes part distortion and preserves the properties of the original material. The compatibility of this technology with robotic arms and rotary table systems facilitates large build volumes and the production of near-net-shape components, thereby reducing material waste and the need for extensive post-processing machining.

Previous studies have extensively investigated SiC/stainless steel microstructures and wear resistance [2,3], as well as laser deposition parameters and performance [1,4–6]. Key references for validation methods include evaluations of non-destructive testing (NDT) in additive manufacturing and coating applications [7,8], alongside performance analysis for industrial nozzle environments [9,10].

This study utilizes DED-LB technology to apply a Silicon Carbide (SiC)-reinforced Metal Matrix Composite (MMC) coating. The objective is to optimize high-value, large-scale industrial sulfur recovery nozzles using a lower-cost substrate [11,12]. The primary innovation of this work lies in achieving a true, defect-free metallurgical bond via precise, computer-controlled, real-time coaxial powder delivery. This approach reduces heat input, thereby minimizing thermal impact and micro-cracking compared to traditional manufacturing techniques. Specifically, this research focuses on the controlled, high-precision application of multi-material coatings with an exceptionally small HAZ. This enables the production of functionally graded layers on critical zones to minimize distortion and material waste while ensuring superior structural integrity compared to traditional methods [13].

2. Materials and Method

The methodology relied on a fully integrated, computer-controlled DED-LB system utilizing a solid-state Rofin Sinar Nd:YAG laser generator (Rofin Sinar, Plymouth, MI, USA) with a maximum power output of 2 kW. Operating at a characteristic near-infrared wavelength of 1064 nm in continuous-wave mode, this laser source ensures excellent energy absorption by metallic substrates and powder feedstocks compared to traditional gas lasers. Beam delivery was executed via a flexible fiber-optic cable routed to a multi-axis robotic deposition head, maintaining a focused spot size of 1.0 mm to achieve a high-density energy profile. This setup created a precise melt pool onto the substrate, into which fine metallic powder was coaxially and continuously injected using argon as an inert carrier and shielding gas. The effective laser beam working area on the substrate was 2.4 mm. The particle feeding equipment consists of a cyclone connected to the shielding gas system, ensuring a constant flow of SiC. To reduce the interaction time between the laser beam and the particles, the laser beam focal point was positioned 6 mm below the substrate surface. This defocusing decreases the laser beam energy density and allows for precise positioning above the surface where the injected particles interact with the beam. These controlled parameters were critical for ensuring strong metallurgical bonding.

To execute the fabrication, a digital workflow was established. First, the part geometry was designed in FreeCAD v1.1 software to generate the toolpath and corresponding G-code. This data was then imported into RoboDK v5.9.5 software, where kinematic simulation and collision checks were conducted [14,15]. During this stage, the Material Deposition function was utilized to virtualize the layer-by-layer material buildup and optimize process variables, such as travel speed and track overlapping. This optimization aimed at the minimisation of HAZ and material waste.

Samples with defined geometry were produced on two types of stainless steels—Avesta 254 SMO (EN 1.4547/X1CrNiMoCuN20-18-7/UNS S31254) (super austenitic stainless steel) [16] and X15CrNiSi25-21 (austenitic stainless steel) [17]. The SiC reinforcement

particles had a size distribution of 45–90 µm. These particles featured an irregular, angular morphology with a nominal purity of 99.0%. Due to the coarse particle size range, the powder exhibited a free-flowing behavior without significant agglomeration, ensuring a consistent and uniform feeding rate during the deposition process.

While conventional applications rely on the standalone properties of uncoated alloys—such as the high pitting resistance of Avesta 254 SMO and the high-temperature oxidation resistance of X15CrNiSi25-21 steel—this study introduces a superior alternative by applying a ceramic SiC-reinforced MMC layer. By transforming these baseline steels into advanced surface composites, the research demonstrates that the fabricated components achieve the required thermal stability and erosion-wear resistance. Furthermore, the application of non-destructive testing confirms that the new AM material is suitable for nozzle fabrication [18,19].

Characterization methods:

Microstructural Analysis—The micro and macrostructure were examined using an Axiovert 200MAT microscope (Carl Zeiss Microscopy GmbH, Jena, Germany) equipped with an Axiovision camera for image recording. Metallographic samples were etched using a mixture of 10 mL HNO_3, 20 mL HCl and 30 mL H_2O. Samples were held in the solution for 15 min and subsequently polished.

Non-destructive testing—Ultrasonic inspection was carried out using a Krautkrämer Branson USD 10 ultrasonic flaw detector (Krautkrämer GmbH, Hürth, Germany). The instrument provides real-time A-scan display visualization for the accurate characterization, localization and evaluation of internal defects within the test samples. Visual testing (VT) was also performed according to standard protocols.

3. Results

To determine the optimal parameters for the DED-LB, a simulation was first conducted, followed by actual implementation. After the solidification process, visual testing (VT) and ultrasonic testing (UT) were applied for non-destructive evaluation to check for disbonding and subsurface imperfections. Subsequently, samples were subjected to microhardness measurements, bond strength tests, microcracking detection, porosity analysis, interface zone assessments and microstructural analysis.

3.1. Simulation

The RoboDK (Robot Development Kit) software (RoboDK, Montreal, QC, Canada), featuring a dedicated robotic additive manufacturing module, was used to perform kinematic simulation of the DED-LB process. The model with the desired geometry was imported from a CAD/CAM system (FreeCAD), and the G-code required for precise movement control was generated. Once the final toolpath was ready, a 3D printing simulation was conducted using the Material Deposition function to accurately visualize the laser-melted powder layering. The visualization of the build-up is shown in Figure 1.

The quantitative validation of the digital workflow was established by directly comparing the ideal pre-programmed toolpath dimensions from the RoboDK simulation against the actual physical measurements of the experimental deposits. For the 14-track single-layer cladding sequence, the digital workflow established a nominal simulated track length of 42.00 mm along the horizontal scanning vector and a total nominal lattice width of 33.00 mm, strictly governed by the track pitch (d = 1.8 mm) and the 25% overlap strategy.

https://doi.org/10.3390/engproc2026145016

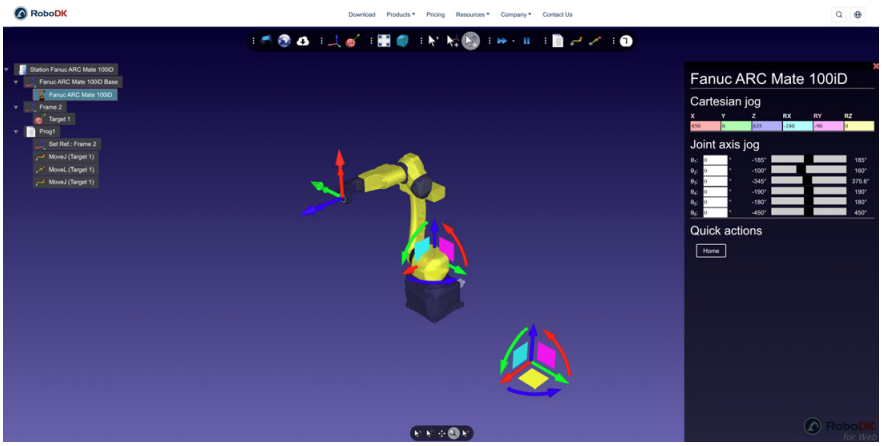


Figure 1. RoboDK Robot Development Kit simulation for AM nozzle structure build-up.

Post-process macroscopic measurements of the physical deposits yielded an actual length of 43.05 mm and an actual total grid width of 34.45 mm. This corresponds to a minimal geometric deviation of +1.05 mm (2.5%) along the horizontal axis and +1.45 mm (4.4%) along the vertical axis. These minor dimensional variances are not execution errors, but provide direct quantitative validation of the process thermodynamics. The robotic system maintained absolute kinematic precision, but the severe interpass heat accumulation within the thin stainless steel substrate—driven by its low thermal conductivity (~15 W/(m·K))—induced significant localized thermal expansion and lateral melt pool wetting. This accumulated thermal load is macroscopically validated by the severe plastic deformation and thermal warping observed in the substrate plate d.

3.2. Part Production via DED-LB

DED-LB was carried out at a power of 1800 W, transverse speed of 1500 mm/min, 25% overlap and powder feed rate of 8 g/min. The process achieved a heat input of 0.4 to 0.7 KJ mm^{-1}. This is the specified overall cumulative target range. The calculation of the energy input (rate) [20–24], named welding energy (E) or heat input (Q), is calculated using Equation (1).

$$E = \frac{P}{v} \quad (1)$$

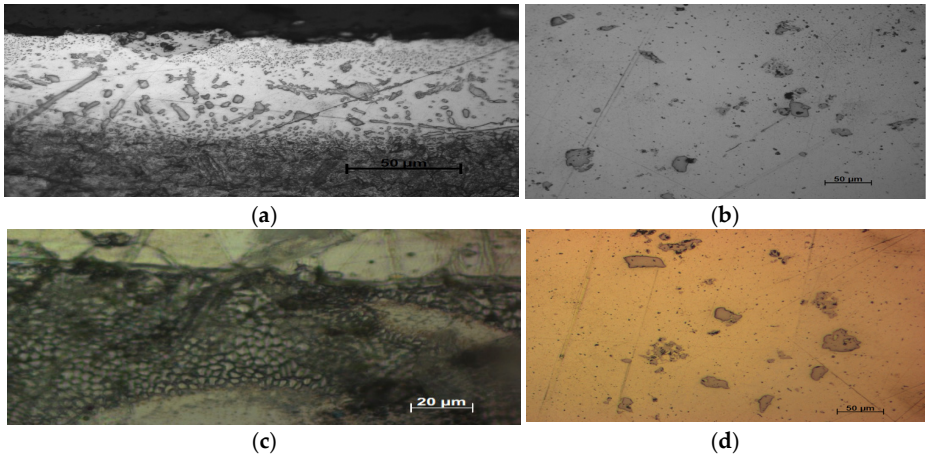
where E = heat input in joules per millimeter (J/mm), P = power in watts (W), v = travel speed in millimeters per minute (mm/min). For a single track, the corresponding result is 0.072 KJ mm^{-1}, considering an efficiency factor (1.0), which is quite theoretical but is in accordance with the standardized methodology for high energy density processes specified in EN 1011-6 [25].

3.3. Microstructure

Since both X15CrNiSi25-21 and Avesta 254 SMO steels belong to the austenitic class, the laser welding zone mainly consists of the weld pool and the heat-affected zone. As seen in Figure 2, the fusion zone contains an austenitic phase characterized by dendritic and cellular formations due to high cooling rates.

It should be noted that the ratio of the temperature gradient to the cooling rate determines the solidification type of the microstructure in the fusion zone. In this case, the ratio is maximum at the fusion boundary and minimum at the weld center. Consequently, locally dispersed cellular structures form at the fusion boundaries, transitioning into dendritic structures towards the weld center due to the decrease in this ratio. A closer examination of the weld pool reveals an increased amount of austenite, which formed

through the coarsening of pre-existing austenitic grain boundaries and intergranular voids. For the thermal reactor nozzles, the surface properties are of relevance. Cumulative microhardness for Avesta 254 SMO with SiC is 240 ± 7.8 HV. The data for the mechanical properties (in Table 1, only for one particular material) are presented below [3].



(**a**) (**b**)

(**c**) (**d**)

Figure 2. AM-produced MMC: (**a**) SiC with X15CrNiSi25-21 surface visualization, (**b**) SiC with X15CrNiSi25-21 internal structure, (**c**) SiC with Avesta 254 SMO surface visualization, (**d**) SiC with Avesta 254 SMO internal structure.

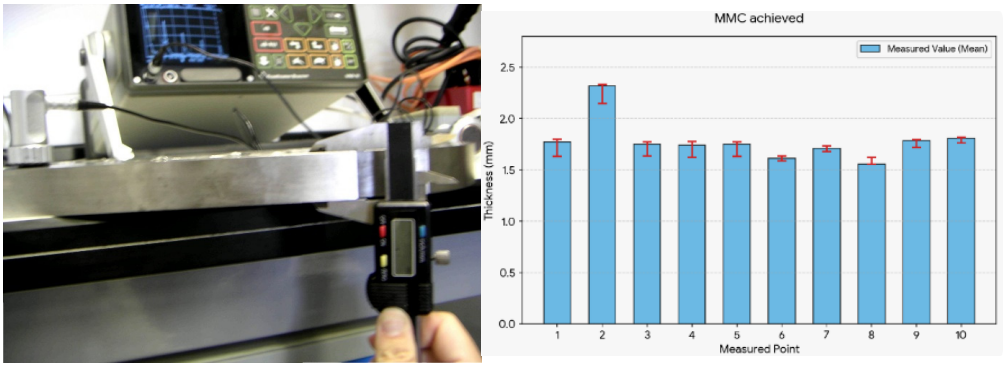
Table 1. Material's characterization—mechanical properties.

Specimen	Coating Thickness (µm)	Yield Strength $R_{p0.2}$ (MPa)	Tensile Strength R_m (MPa)	Hardness HBV1	Porosity (%)
Avesta 254 SMO + SiC	550	601.0	747.6	240 ± 7.8 HV	1.57

3.4. Non-Destructive Evaluation

Visual inspection of the samples of Avesta 254 SMO + SiC was carried out, and no defects were identified in accordance with EN ISO 17637 [26].

Ultrasonic inspection was performed and no discontinuities were detected in accordance with EN ISO 17640 [27]. Consequently, the quality of the obtained samples was found to be acceptable according to the acceptance level C of EN ISO 11666 [28]. Figure 3 illustrates the UT process (for the investigated lot of samples, only the overall achieved MMC is reported, accounting for the waving pattern on top).



(**a**) (**b**)

Figure 3. Ultrasonic testing of the Avesta 254 SMO + SiC: (**a**) calibration of the equipment and (**b**) summary of data obtained and evaluated.

A standard carbon steel No. 1 (V1) calibration block was used for the baseline setup of the ultrasonic flaw detector, including time base adjustments and transducer index verification. Following this baseline calibration, systematic measurements were performed on stainless steel components using a specialized ultrasonic probe. To compensate for the acoustic velocity mismatch between the carbon steel reference block and the stainless steel + SiC specimens, the instrument's velocity settings were adjusted to match the stainless steel matrix, ensuring precise sound path calculations across all utilized transducers. The experimental evaluation focused on four critical metallurgical parameters, conducted via conventional ultrasonic testing (UT) using a Krautkrämer Branson USD 10 digital flaw detector. High-resolution RF signals were monitored via live A-scan displays using a 10 MHz dual-element straight-beam transducer (DA312, with a Ø7.5 mm element size, an operating range of 0.6–50 mm, and a temperature rating of t < 60 °C).

Bond strength: The amplitude of the interface echo on the A-scan was continuously monitored; the complete absence of a boundary reflection confirmed a fully fused, high-strength metallurgical joint with optimal structural continuity.

Microcracking detection: The material was confirmed free of sub-surface microfissures, demonstrating the high-resolution capability of the 10 MHz longitudinal waves to identify even minor acoustic discontinuities.

Porosity: No volumetric porosity or gas entrapment was detected within the analyzed zones. To maintain rigorous detection sensitivity, the USD 10 instrument was calibrated at a gain of 46 dB, with the monitoring gate (Gate A) configured at a start (A-strt) of 0.97, a width (A-wdth) of 50.0 and a threshold amplitude (A-thr) of 50%. The total absence of structural noise or defect echoes exceeding this 50% threshold verified a defect-free MMC.

Interface-zone assessment: The structural integrity across the transition layer was validated by the steady uniformity of the back-wall echo sequence, confirming excellent acoustic homogeneity and stable sound transmission throughout the fused boundary.

4. Discussion

The successful fabrication of SiC-reinforced Metal Matrix Composites (MMCs) on austenitic stainless steel substrates via Directed Energy Deposition-Laser Beam (DED-LB) demonstrates the viability of this process for enhancing the surface properties of critical industrial components. The discussion below analyzes the metallurgical outcomes, the efficacy of the non-destructive testing (NDT) protocols, and the comparative advantages of this approach over conventional manufacturing methods.

4.1. Metallurgical Bonding and Microstructural Integrity

A primary challenge in laser cladding of ceramic-reinforced composites is achieving a strong metallurgical bond without inducing excessive dilution or brittle intermetallic phases. In this study, the absence of disbonding and subsurface imperfections, as confirmed by ultrasonic testing (UT), indicates that the optimized heat input was sufficient to melt the substrate surface and the incoming powder simultaneously, ensuring atomic-level diffusion at the interface.

The microstructural analysis revealed a transition from cellular structures at the fusion boundary to dendritic structures toward the weld center. This morphology is characteristic of rapid solidification processes where the temperature gradient and solidification rate vary spatially within the melt pool [1,4]. The presence of dispersed SiC particles within the austenitic matrix contributes to the observed increase in hardness. The SiC particles act as reinforcement agents, hindering dislocation movement and thereby improving wear resistance. However, the relatively low porosity (1.57%) suggests that the shielding gas

flow and powder feed rate were well-balanced, minimizing gas entrapment—a common defect in powder-based AM processes [7,8].

4.2. Efficacy of Non-Destructive Evaluation

The integration of visual testing (VT) and ultrasonic testing (UT) provided a robust quality assurance framework. The use of a 10 MHz dual-element transducer allowed for high-resolution detection of micro-defects. The absence of interface echoes in the A-scan data confirms a continuous metallurgical bond, which is critical for components subjected to high thermal and mechanical fatigue, such as sulfur recovery nozzles.

Compared to traditional welding methods, DED-LB offers a significantly smaller heat-affected zone (HAZ), reducing the risk of thermal distortion and grain coarsening in the base material [13]. The UT results validate that the process parameters can be controlled to produce industrial-grade parts without the need for destructive sampling for every unit. This is particularly advantageous for large-scale nozzle manufacturing, where maintaining dimensional accuracy is paramount.

4.3. Comparative Advantages and Industrial Relevance

The application of SiC-reinforced MMCs on lower-cost austenitic steels (X15CrNiSi25-21 and Avesta 254 SMO) presents a cost-effective alternative to using fully exotic superalloys for the entire component. By applying the high-performance composite layer only to the erosion-prone outer surface, material costs are reduced while extending the service life of the nozzle in harsh environments characterized by high friction and thermal stress [9,10] and precise control over the deposition process. The minimal geometric deviation between the simulated and actual parts highlights the reliability of the robotic system. This predictability is essential for scaling the process to industrial production, where consistency and repeatability are key [14,15].

4.4. Limitations and Future Work

While the current study demonstrates successful bonding and improved hardness, further investigation is required to evaluate the long-term erosion-corrosion resistance of the MMC coating under actual operating conditions. Future work should include:

Tribological testing: quantitative analysis of wear rates under simulated sulfur recovery conditions.

Thermal cycling: assessment of the coating's integrity after repeated thermal shocks to identify potential thermal fatigue cracks.

Multi-layer deposition: investigation of residual stress accumulation in thicker coatings, which may require interlayer cooling strategies or post-process heat treatment.

5. Conclusions

The successful DED-LB fabrication of a defect-free, SiC-reinforced MMC layer on stainless steel provides a durable and cost-effective solution for upgrading sulfur recovery thermal reactor nozzles.

Experimentally verified is the structural integrity and defect-free nature of the fabricated coatings. Simulation compared to experimental application of AM layers shows a minimal geometric deviation of +1.05 mm (2.5%) along the horizontal axis and +1.45 mm (4.4%) along the vertical axis. The achieved base with Avesta 254 SMO + SiC is between 1.56 (+0.07/−0.00) and 2.32 (+0.01/−0.17) mm. Subsequent non-destructive evaluations (VT and UT) confirmed no defects and strong metallurgical bonding. Further high-temperature erosion testing, residual-stress measurement and different multi-layer functionally graded coatings could be planned for investigation. But the present com-

bined findings demonstrate that the developed new composite structure is suitable for the successful upgrade of sulfur recovery thermal reactor nozzles.

Funding: This research was funded by the European Regional Development Fund under the Operational Program "Scientific Research, Innovation and Digitization for Smart Transformation 2021–2027", Project CoC "Smart Mechatronics, Eco- and Energy Saving Systems and Technologies", BG16RFPR002-1.014-0005.

Institutional Review Board Statement: Not applicable.

Informed Consent Statement: Not applicable.

Data Availability Statement: The data is contained within the article.

Acknowledgments: The author would like to express gratitude to the University "Prof. Dr. Assen Zlatarov" Burgas, Bulgaria, Technischen Universität Chemnitz, Germany and the Open Laboratory on Experimental Micro and Nano Mechanics (OLEM), Bulgaria.

Conflicts of Interest: The author declares no conflicts of interest.

References

1. Ostolaza, M.; Arrizubieta, J.I.; Lamikiz, A.; Plaza, S.; Ortega, N. Latest Developments to Manufacture Metal Matrix Composites and Functionally Graded Materials through AM: A State-of-the-Art Review. *Materials* **2023**, *16*, 1746. [CrossRef] [PubMed]
2. Mussatto, A.; Ahad, I.U.; Mousavian, R.T.; Delauré, Y.; Brabazon, D. Advanced production routes for metal matrix composites. *Eng. Rep.* **2021**, *3*, e12330. [CrossRef]
3. Boshnakova, S. Method for Additive Manufacturing of Steel Components with Enhanced Surfaces Properties in the Automotive Sector. *Phys. Sci. Forum* **2026**, *15*, 3. [CrossRef]
4. Zhou, Y.; Ning, F. Directed energy deposition of SS 316L/SiC composites using coincident and coaxial wire-powder feeding. *Mater. Lett.* **2023**, *35*, 557–563. [CrossRef]
5. Boshnakova, S.; Rusev, D.; Markovska, I. Si-Metal Composites Strengthening Mechanism. *J. Chem. Technol. Metall.* **2015**, *50*, 557–560.
6. Ubaldini, S. Advanced Technologies in Bio/Hydrometallurgy for Recovery and Recycling of Metals. *Metals* **2023**, *13*, 1105. [CrossRef]
7. Wang, P.; Zeng, J.; Lou, D.; Zheng, W.; Zheng, S.; Chen, B.; Gao, Z. Nonlinear Ultrasonic Characterization of Processing Defects in Wire Arc Additive Manufacturing 316L Stainless Steel. *Materials* **2025**, *18*, 805. [CrossRef] [PubMed]
8. Singh, G.; Yu, J.; Xu, F.; Yao, T.; Xu, P. Multiscale Modeling of Silicon Carbide Cladding for Nuclear Applications: Thermal Performance Modeling. *Energies* **2024**, *17*, 6124. [CrossRef]
9. Honarvar, F.; Varvani-Farahani, A. A review of ultrasonic testing applications in additive manufacturing: Defect evaluation, material characterization, and process control. *Ultrasonics* **2020**, *108*, 106227. [CrossRef] [PubMed]
10. Serrati, D.S.M.; Machado, M.A.; Oliveira, J.P.; Santos, T.G. Non-Destructive Testing Inspection for Metal Components Produced Using Wire and Arc Additive Manufacturing. *Metals* **2023**, *13*, 648. [CrossRef]
11. Boshnakova, S.; Markovska, I.; Rusev, D. SiC and TiC Stainless Steel Based Metal Matrix Composites. *Sci. Work Ruse Univ.* **2015**, *54*, 14–18.
12. Chaudhary, R.; Akbari, R.; Antonini, C. Rational Design and Characterization of Materials for Optimized Additive Manufacturing by Digital Light Processing. *Polymers* **2023**, *15*, 287. [CrossRef] [PubMed]
13. Boshnakova, S. Manufacturing Technologies Comparison for Nozzles. *Eng. Proc.* **2026**, *150*, 68. [CrossRef]
14. RoboDK Inc. RoboDK: Simulator for Robot Arms and Offline Programming. Available online: https://robodk.com/ (accessed on 22 June 2026).
15. RoboDK Documentation. Robot Simulation and Offline Programming Application Examples: Welding and Additive Manufacturing. Available online: https://robodk.com/simulation (accessed on 22 June 2026).
16. *EN 10088-4*; Stainless Steels—Part 4: Technical Delivery Conditions for Sheet/Plate and Strip of Corrosion Resisting Steels for Construction Purposes. CEN: Brussels, Belgium, 2014.
17. *EN 10095:1999*; Heat Resisting Steels and Nickel Alloys. CEN: Brussels, Belgium, 1999.
18. Bilici, V.Ö. Investigation of physical and metallographic properties of nickel matrix composite by ultrasonic method. *J. Radiat. Res. Appl. Sci.* **2024**, *17*, 100894. [CrossRef]
19. Oliveira, T.L.L.; Hadded, M.; Mimouni, S.; Schaan, R.B. The Role of Non-Destructive Testing of Composite Materials for Aerospace Applications. *NDT* **2025**, *3*, 3. [CrossRef]

20. Steen, W.; Mazumder, J. *Laser Material Processing*, 4th ed.; Springer: London, UK, 2010.
21. Toyserkani, E.; Khajepour, A.; Corbin, S. *Laser Cladding*; CRC Press: Boca Raton, FL, USA, 2004.
22. Picasso, M.; Marsden, C.F.; Wagniere, J.-D.; Frenk, A.; Rappaz, M. A simple but realistic model for laser cladding. *Metall. Mater. Trans. B* **1994**, *25*, 281–291. [CrossRef]
23. Ion, J. *Laser Processing of Engineering Materials*; Elsevier: Oxford, UK, 2005.
24. Siltanen, J. Laser and Hybrid Welding of High-Strength Structural Steels. Ph.D. Thesis, Lappeenranta-Lahti University of Technology LUT, Lappeenranta, Finland, 2023.
25. *EN 1011-6*; Welding—Recommendations for Welding of Metallic Materials—Part 6: Laser Beam Welding. CEN: Brussels, Belgium, 2018.
26. *EN ISO 17637*; Non-Destructive Testing of Welds—Visual Testing of Fusion-Welded Joints. ISO: Geneva, Switzerland, 2016.
27. *EN ISO 17640:2018*; Non-Destructive Testing of Welds—Ultrasonic Testing—Techniques, Testing Levels, and Assessment. ISO: Geneva, Switzerland, 2018.
28. *EN ISO 11666:2018*; Non-Destructive Testing of Welds—Ultrasonic Testing—Acceptance Levels. CEN: Brussels, Belgium, 2018.

Disclaimer/Publisher's Note: The statements, opinions and data contained in all publications are solely those of the individual author(s) and contributor(s) and not of MDPI and/or the editor(s). MDPI and/or the editor(s) disclaim responsibility for any injury to people or property resulting from any ideas, methods, instructions or products referred to in the content.